Journal of Non-Crystalline Solids 531 (2020) 119853

Contents lists available at ScienceDirect

Journal of Non-Crystalline Solids

journal homepage: www.elsevier.com/locate/jnoncrysol

Physical and optical properties of a-Ge-Sb-Se-Te bulk and film samples: Refractive index and its association with electronic polarizability of thermally evaporated a-$Ge_{15-x}Sb_xSe_{50}Te_{35}$ thin-films

Ahmed Saeed Hassanien[a,b,*], Ishu Sharma[c], Alaa A. Akl[d,e]

[a] Engineering Mathematics and Physics Department, Faculty of Engineering at Shoubra - Cairo, 11629, Benha University, Egypt
[b] Physics Department, Faculty of Science and Humanities in Afif, 11921, Shaqra University, Saudi Arabia
[c] Department of Physics, Amity University Dubai, Dubai, United Arab Emirates
[d] Physics Department, Faculty of Science Minia University, Egypt
[e] Physics Department, Faculty of Science and Humanities in Dawadmi, 11911, Shaqra University, Saudi Arabia

ARTICLE INFO

Keywords:
Amorphous semiconductors
Quaternary chalcogenides
Bulk and thin films
Physical properties
Electronic polarizability
Average heat of atomization

ABSTRACT

This work is dedicated to the deduction of many basic physical parameters of a-$Ge_{15-x}Sb_xSe_{50}Te_{35}$ bulk and thin-film samples, GSST ($0.0 \leq x \leq 15.0$ at.wt.%). Besides, study the interrelationships among refractive index, molar refractivity and electronic polarizability of these film samples. Solid-state solutions of GSST compositions were prepared followed by melt-quenching method to get the glassy bulk samples. The thin-film samples of thickness 200 nm were fabricated by thermal evaporation technique. X-ray diffractograms revealed that all prepared GSST bulk and film samples are of non-crystalline nature. The ingots bulk Ge-Sb-Se-Te samples have been used to practically estimate the density. The refractive index of $Ge_{15-x}Sb_xSe_{50}Te_{35}$ amorphous thin-films have been utilized to discuss the electronic polarizability, Covalence parameter and optical electronegativity. As well as, the deviation from stoichiometry, average heat of atomization, the overall mean bond energy and the glass transition temperature are also evaluated. All studied parameters are highly dependent on the Sb-ratio.

1. Introduction

Chalcogenide glasses contain one or more of the chalcogen elements, like S, Se, Te and are covalently linked to the elements/metals viz. Ge, In, As, Sn, Bi, Sb, etc. The chalcogenide metal-doped glasses have become an essential class of non-crystalline semiconductor industry. The revelation of superb transmission in near and far IR spectral region allows these materials to have a significant role in the field of optoelectronics [1–4]. These alloys are vibrant due to their new and distinctive properties viz. low phonon energy, excellent transmittance range, wider bandgap, high linear, non-linear refractive index, etc. Therefore, they have wide usage in IR sensors, photo-detectors, LED, waveguides, holography and others [1,5–7]. Chalcogenides are high refractive index materials and also show high non-linearity almost $\approx 10^2$ times of silica [8] and are used as an ultrafast switch [9,10]. Fabrication of optical devices is easy with chalcogenide materials owing to their high thermal and chemical stability [11–15]. Metallic doping in chalcogens based matrix changes the average coordination number and bring structural changes, i.e. flexible ↔ intermediate ↔ rigid in the network. Therefore, physical and optical properties can be modified in a controlled manner, as per industry requirement [16,17].

Among chalcogenides, the pure selenium element has always been one of the preferred host matrix owing to its high glass-forming ability [18] and great commercial importance in xerography. Nonetheless, pure Se shows some limitations like low sensitivity and short lifetime. To get over this limitation, researchers alloy Se with few preferred additives (Ge, Te, Bi, Sn, Cd, Sb, etc.) [19–21]. Similar to Se, pure Te has the poor glass-forming ability, but in spite of this limitation shows a wide IR transparency window, high refractive index, display phase change and has excellent non-linear properties. In the present investigation, Se-Te has been chosen as a fundamental host matrix, with modified properties, i.e., comparatively high photosensitivity, hardness, improved aging effect and higher crystallization temperature [22,23]. The features depict be Se-Te binary composition can be improved by the addition of the third element which can enhance the application domain. In the present work, Ge is chosen as the third component in the network. Addition of Ge further enhances glass forming region, thermal stability and lessen aging effects as Ge makes

* Corresponding author.
E-mail addresses: ahmed.hassanien@feng.bu.edu.eg (A.S. Hassanien), alaaakl2010@windowslive.com (A.A. Akl).

https://doi.org/10.1016/j.jnoncrysol.2019.119853
Received 23 September 2019; Received in revised form 23 November 2019; Accepted 5 December 2019
Available online 24 December 2019

crosslinking with Se chains, thereby strengthening the system's average bond, thus, and acts as a bond modifier. Even the compatible size and electronegativity values of Ge produce highly stable glassy melt [21–23].

The authors have already studied electrical, optical, structural, physical and thermal properties of various ternary, quaternary chalcogenide glassy system viz, Cd-S-Se, Ge-Se, Se-Zn, Ge-Te, Ge-Se-Te with different metallic doping; In, Bi, Sb, etc.[24–30] and come out with various industries oriented results. In the present work, $Ge_{15}Se_{50}Te_{35}$ is kept as a base matrix and authors aim to study the effect of Sb as a dopant, in Ge-Se-Te network. Optical and few physical properties of t GSST amorphous samples have already been studied in previous work [31,32].

Changes in optical and physical parameters hint towards the fact that new defects are being created in the network with Ge substitution by Sb. Therefore, it affects the short- and medium-range order in the films which further results in the tailoring of the properties. Adding Bi and Sb unpin Fermi level and support carrier-type reversal in the matrix, i.e. p ↔ n and therefore, helps in enlarging the glassy region of the network, enhances thermal stability and increases IR transmission. Therefore, Sb-doped Ge-Se-Te glasses are a remarkable multi-functional material for plentiful applications [33–35]. It is also worth mentioning that the antimony is used as a chemical modifier, as well as it causes compositional and configurational disorders and hence, an amendment in the structures of the chemical composition is expected, keeping in mind the application or device itself [33,34].

In recent work, it was observed that the Sb-addition in the Ge-Se-Te host lattice improves thermal properties, which in turn leads to an increase in refractive index (n) values [31,32]. Besides this, the authors are also carrying out a comprehensive study for several optical properties due to distinguished benefits and crucial advantages. Therefore, the present work is a continuation of previously published work [31,32]. The authors have decided to evaluate the density experimentally and its correlated parameters, and to study extensively the electronic polarizability and optical electronegativity, as well as some other crucial parameters.

Therefore, the present manuscript aims to comprehend and discuss some essential physical parameters of $Ge_{15-x}Sb_xSe_{50}Te_{35}$ (x = 0, 4, 8, 12, 15 at.%) glassy alloys and to study the interrelationships among the parameters of GSST glassy **system and respective** film samples. This manuscript is considered as a significant study of the basic physical concepts from an application point of view. In this work, the impact of the substitution of Ge by Sb in a-Ge-Sb-Se-Te quaternary alloys on the physical properties of each sample of $Ge_{15-x}Sb_xSe_{50}Te_{35}$ matrix (x = 0, 4, 8, 12, 15 at.%) are studied and discussed. Here, the mass-volume density, of the prepared chalcogenide matrix, has been experimentally measured using the Archimedes principle technique and also estimated theoretically Besides, several related parameters such as molar mass, free volume percentage, compactness and many others have also been investigated for each composition. Moreover, to know about the nature of the chemical bonds in the present amorphous GSST bulk and film samples, optical electronegativity is studied, the non-linear response is also governed by the optical electronegativity. Besides, molar reflectivity, reflection loss, Covalence parameters are also calculated and discussed. Moreover, the increase in refractive index values is discussed based on electronic polarizability, which is calculated using two models and then compared.

Table 1 summarizes the most important characteristics of elements of the GSST glassy network used for investigating the target parameters [36–38].

2. Experimental detail

2.1. Synthesis of glassy alloys and thin-film samples

Conventional melt-quenching technique was used to carry out the synthesis process of quaternary bulk $Ge_{15-x}Sb_xSe_{35}Te_{50}$ (x = 0, 4, 8, 12, 15 at.%) glasses. Elements were weighted according to their atomic weight percentage and sealed in an evacuated quartz ampoule ($\approx 10^{-4}$ Pa). The sealed ampoules were heated to 1100 °C in step heating with an approximate rate of 3–4°C. Before the ice-water quenching, the temperature of samples within the oven was fixed constant at 1100°C for 18 h.

All heat treatments, such as gradual and lower heating rate (3–4°C/h) of furnance, continuously rocking the samples stabilizing the temperature of furnace at 1100°C, ensure good homogeneity of the molten mixture. Thin-film samples of quaternary $Ge_{15-x}Sb_xSe_{50}Te_3$ glassy alloys were prepared by the thermal evaporation technique using Edwards E-306A vacuum coating-unit under a vacuum $\approx 8.2 \times 10^{-4}$ Pa. Ultrasonically cleaned KH-microscopic glass slides were used as a substrate for the fabrication of films. The transparent glass slides have better optical quality and a high degree of purity [39,40].

For thin-film fabrication, pre-cleaned molybdenum boat was used. Before the start of the deposition process of films, a heavy current was passed through the boat to pre-clean it, until it became red hot. Then, after the current was passed slowly and increased gradually through the boat until film [is deposited] onto the substrate. The film thickness was monitored and controlled by a quartz crystal oscillator, QCO (Edward), embedded near to the utilized substrate.

2.2. Characterization and measurement of samples

X-ray diffractometer “JEOL - Model JSDX-60PA” was used to affirm the amorphous/crystalline nature of the thin-film samples of GSST samples. This diffractometer was adjusted to operate at an electric current of $\approx$ 35 mA and voltage $\approx$ 40 kV. The used source of the radiation was Cu-k_α, which has energy equals to 8.042 keV and the average wavelength of 1.54184 Å. A slow scan and continuous counting rate (1^0/min), besides a small-time constant (1 s) were applied to examine each GSST sample in the angular range (2θ) that extended from $6o^0$ to 85^0. These specifications make the diffractometer able to detect any possible diffracted lines [41]. All X-ray diffraction patterns were examined at room temperature. The absence of a sharp diffraction peak confirms the amorphous nature of the examined sample.

Moreover, for compositional analysis of the amorphous quaternary $Ge_{15-x}Sb_xSe_{50}Te_{35}$ network energy-dispersion X-ray spectroscopy technique was used. The unit of EDX was interfaced with the SEM, which was operated with 30 kV. Different places at the surface of the sample were scanned and analyzed more than three times, to get accurate values of the elements' ratios. The error in the ratios of the elements of any composition was found to be less than $\pm$ 1.0%.

A double beam spectrometer of Shimadzu UV–Vis-NIR (UV 3101-PC) was used to measure and analyze the optical transmission, T and the reflection, R spectra of the thin film, as functions of the wavelength in the spectral range of 200 nm to 2500 nm. The spectrophotometer is equipped with a reflection attachment with V-N type (incident angle 5°). Moreover, it has two sets of three gratings to cover the wide range of the incident light, that extended from the UV to the N-IR regions, which almost gives fixed energy and signal-to-noise. The measurement baseline is performed using two cleaned glass substrates (similar to those used for film fabrication) situated through the spectrophotometer beams. Hence, the accuracy of the measured T and R spectra of present GSST film samples as recorded by the spectrophotometer is as low as 1%.

2.3. Mass-volume density and determination of some related parameters

The ingots bulk chalcogenide samples have been used to measure the mass-volume density for each composition, experimentally. Archimedes principle is used to evaluate the density value of each chalcogenide composition as given [4,42]:

Table 1.
Some used parameters of elements of synthesized $Ge_{15-x}Sb_xSe_{50}Te_{35}$ samples [36–38].

Element	Density (gm/cm^3)	Molar Mass (gm/mol)	Molar volume (cm^3/mol)	Atomic density (atom/cm^3) × 10^{22}	Electro negativity (Pauling scale)	Coordination number, <CN>	Optical energy gap (eV)	Heat of atomization, H_s kCal/g.atom
Ge	5.32	72.63	13.63	4.419	2.01	4	0.67	90.0
Sb	6.69	121.76	18.19	3.311	2.05	3	0.00	62.0
Se	4.97	78.97	16.42	3.668	2.55	2	1.74	49,4
Te	6.24	127.60	20.46	2.944	2.10	2	0.34	46.0

$$\rho = \rho_t\left(\frac{W_a}{W_a - W_t}\right) \quad (1)$$

Where ρ_t is the toluene liquid density (used as the buoyant liquid), W_a and W_t are the own weight of the bulk $Ge_{15-x}Sb_xSe_{50}Te_{35}$ glassy sample in air and toluene, respectively. The density of each bulk sample has been experimentally measured at least four times under the same applied practical conditions and then their mean values are taken. The density of each bulk $Ge_{15-x}Sb_xSe_{35}Te_{50}$ (x = 0, 4, 8, 12, 15) sample is also theoretically calculated and a comparison between the theoretical and experimental density results is reported, as listed in Table 3. The error in the experimental values of the measured density is within the value ± 0.024 gm/cm^3. By knowing the density and molar mass, the molar volume, V_M of each bulk sample is determined as follows [4,43]:

$$VM = \frac{1}{\rho_{Exp}}\sum x_i M_m \quad (2)$$

Where ρ_{Exp} is the experimentally measured density, and $\Sigma x_i M_m$ is the resultant molar mass of each chalcogenide Ge-Sb-SeTe bulk sample, which is calculated from the following relation [44]:

$$\sum x_i M_m = \alpha M_m - Ge + \beta M_m - Sb + \gamma M_m - Se + \delta M_m - Te \quad (3)$$

Where, α, β, γ and δ are the atomic percentage (atomic fraction) of the presence of Ge, Sb, Se and Te in the composition, while M_m-Ge, M_m-Sb, M_m-Se and M_m-Te are the molar masses of Ge, Sb, Se and Te, respectively. The accuracy of the calculated values of the molar volume of the sample in comparison to the theoretical values is about ± 0.13 cm^3/mol. There is another quantity related to molar volume, which is the excess volume, V_e. It is calculated from the following equation [4,44]:

$$V_e = V_M - V_T \quad and \quad V_T = \sum_i x_i V_m(i) \quad (4)$$

Where, V_m is the experimentally measured molar-volume of the bulk sample, while V_T is the theoretically calculated value of each sample, which can be estimated as follows [44]:

$$V_T = \alpha V_m(Ge) + \beta V_m(Sb) + \gamma V_m(Se) + \delta V_m(Te) \quad (5)$$

Where, V_m (Ge), V_m (Sb), V_m (Se) and V_m (Te) are the measures of the molar volume of Ge, Sb, Se and Te, respectively, x_i is the atomic % age of the constituent elements of the sample and $V_m(i)$ represents the molar volume of the respective element present. Consequently, the percentage of free volume, PFV in each sample can be determined by the given formula [44,45]:

$$PFV = \frac{V_M - V_T}{V_M}\ 100\% \quad (6)$$

Depending upon the measured density values, compactness, δ is also calculated and is very significant property. This parameter determines the variation in the mean atomic volume of the substance owing to the mutual chemical interactions between the constituents of the glassy network. Compactness can be estimated for any non-crystalline structure, knowing the values of the percentage of each element in the composition (atomic fraction), x_i, the molar mass $(M_m)_i$ and the atomic density, ρ_i of each element, as well as the atomic density of the composition, ρ. The value of compactness is determined from the given formula [4,46]:

$$\delta = \left[\frac{\sum_i \frac{x_i(M_m)_i}{\rho_i} - \sum_i \frac{x_i(M_m)_i}{\rho}}{\sum_i \frac{x_i(M_m)_i}{\rho}}\right] \quad (7)$$

The packing density, P_D of each compositional sample is another parameter depending on the density. It is known as the ratio between the utilized spaces to the specified space, and it is also given as Avogadro's constant divided by the molar volume of the sample as given by this formula [44,47]:

$$PD = \frac{\rho_{Exp} N_A}{M_m} = \frac{N_A}{V_m} \quad (8)$$

Where ρ_{Exp} is the experimental density value of a given sample, N_A is Avogadro' number, as well as M_m and V_m are the molar mass and molar volume of that sample.

3. Results and discussion

3.1. Structure and EDX studies

Fig. 1 shows the X-ray diffraction schemes for Ge-Sb-Se-Te film samples. As noted, all thin films are free of discrete or sharp lines, therefore depicts an amorphous nature. This result was expected as the deposition rate was 10 nm /S on glass substrate. Moreover, the prepared films are thin (200 nm). It should be noted that XRD-patterns have two humps at different locations from the diffraction angle. These stepped humps have been observed at (2θ) ≈ 15–35° and ≈ 45–55°, which were produced owing to the amorphous nature of the used substrates [14,31,32].

The compositional analysis was studied using the energy-dispersive-X-ray Spectroscopy. The estimated elemental ratio indicated a good agreement between the measured and selected values. Table 2 reports the obtained EDX values. Furthermore, for more details about the X-ray patterns and the elemental EDX-ratios of GSST samples, it is possible to refer to the previously published work [31,32].

3.2. Determination of mass-volume density and its associated parameters

The volume-mass density, ρ is an essential and sensitive parameter and has a great influence on the various physical properties of any material, viz. the transparency, reflectivity, refractive index, thermal conductivity, etc. Both variations in geometrical arrangements, the interstitial spaces and the coordination number of the alloys strongly affect the density values. Therefore, any change in the density value will indicate the occurrence of structural deviations within the glassy material. Consequently, measuring density and studying its relationship with other physical variables is indeed an important topic. Archimedes' principle was used to measure the experimental density values at the room temperature. Moreover, the density values of the present GSST bulk samples were calculated theoretically and a comparison between the experimental and theoretical values was studied. The comparative process was in a good agreement between the measured values in practice and the theoretically calculated ones. The measured and estimated values are reported in Table 3. Experimentally measured density values are also represented in Fig. 2-a. A linear increment from

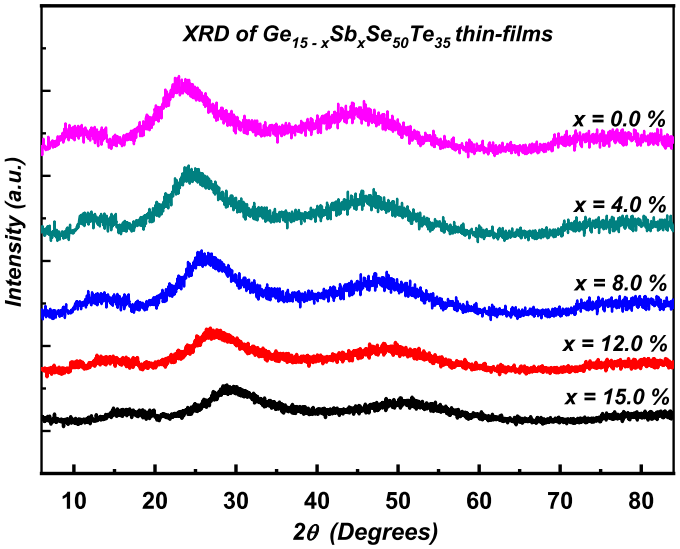

Fig. 1. XRD-patterns of the quaternary $Ge_{15-x}Sb_xSe_{50}Te_{35}$ film samples (x = 0, 4, 8, 12, 15 at.%).

Table 2
The experimentally EDX elemental ratios of $Ge_{15-x}Sb_xSe_{50}Te_{35}$ samples (at.%), [31].

Sample	*EDX (Atomicratio %)*			
	Ge	Sb	Se	Te
$Ge_{15}Se_{50}Te_{35}$	14.70	00.00	51.38	34.02
$Ge_{11}Sb_4Se_{50}Te_{35}$	10.96	3.90	49.05	36.09
$Ge_7Sb_8Se_{50}Te_{35}$	7.53	8.06	48.48	35.93
$Ge_3Sb_{12}Se_{50}Te_{35}$	2.84	11.87	51.03	34.26
$Sb_{15}Se_{50}Te_{35}$	00.00	15.02	49.87	35.11

5.381 gm/cm^3 to 5.597 gm/cm^3 is observed in density values with Sb addition.

Presumably, this increase in density values with Sb addition is due to the fact that both the density and the atomic mass values of the pure antimony are larger than those of pure germanium. The linear equation that links between the density values and the Sb-percentage is given as:

$$\rho_{Exp} = 5.38 + 0.0154x \quad (gm/cm^3) \tag{9}$$

Where, x is the Sb-percentage within the chalcogenide bulk $Ge_{15-x}Sb_xSe_{35}Te_{50}$ glasses. The molar volume, V_m and molar mass, M_m of the prepared $Ge_{15-x}Sb_xSe_{35}Te_{50}$ glasses are also calculated using Eq. (2).

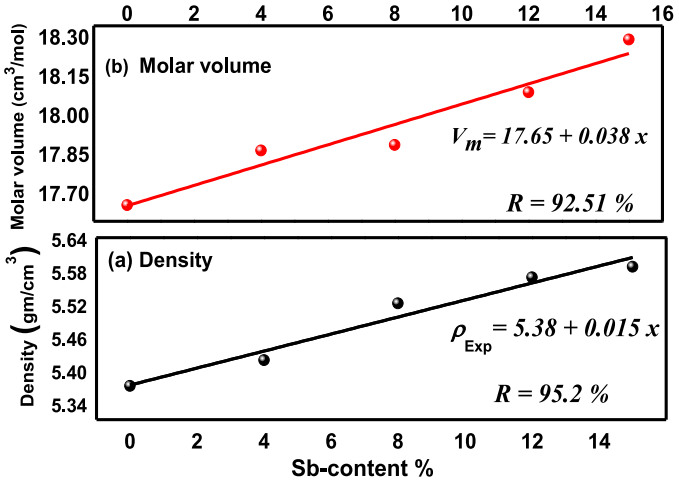

Fig. 2. The variation of both the density, ρ and the molar volume, V_m as a function of the Sb-concentration percentage of the chalcogenide $Ge_{15-x}Sb_xSe_{50}Te_{35}$ glassy matrix.

Table 3
Estimated parameters of the non-crystalline chalcogenide $Ge_{15-x}Sb_xSe_{50}Te_{35}$ glassy samples.

The parameter	Chalcogenide $Ge_{15-x}Sb_xSe_{50}Te_{35}$ glassy composition				
	x = 0.0	*x = 4.0*	*x = 8.0*	*x = 12.0*	*x = 15.0*
Experimental density, ρ_{exp} ± 0.01 (gm/cm^3)	5.381	5.428	5.531	5.578	5.597
Theoretically calculated density, ρ_{th} (gm/cm^3)	5.406	5.465	5.509	5.569	5.609
Molar mass, M_m ± 1.35 (cm^3/mol)	95.040	97.005	98.970	100.935	102.409
Molar volume, V_m ± 0.13 (cm^3/mol)	17.662	17.870	17.893	18.095	18.297
Theoretical molar volume, V_T (cm^3/mol)	17.416	17.598	17.780	17.963	18.100
Excess volume, $V_e = V_m - V_T$ (cm^3/mol)	0.246	0.273	0.113	0.132	0.197
Free volume percentage, *FVP* (%)	1.39	1.43	0.89	0.73	0.89
Packing density, $P_D \times 10^{22}$ (Atom/cm^3)	3.410	3.370	3.366	3.329	3.291
The compactness of the system, δ	−0.029	−0.026	−0.023	−0.021	−0.019
Atomic density of *Sb*, $N_{Sb} \times 10^{21}$ (Atom/cm^3)	0	1.042	2.166	3.342	4.259
Atomic density of *Ge*, $N_{Ge} \times 10^{21}$ (Atom/cm^3)	6.361	4.802	3.177	1.401	0.00
Atomic density, $N \times 10^{22}$ (Atom/cm^3)	1.962	2.008	2.087	2.147	2.186
Se-Se interatomic distance, *SIAD* (Å)	3.71	3.68	3.63	3.60	3.58
The polaron radius, *Rp* (Å)	1.495	1.483	1.463	1.451	1.442
The field strength, $F \times 10^{15}$ (cm^{-2})	8.948	9.093	9.344	9.499	9.6183

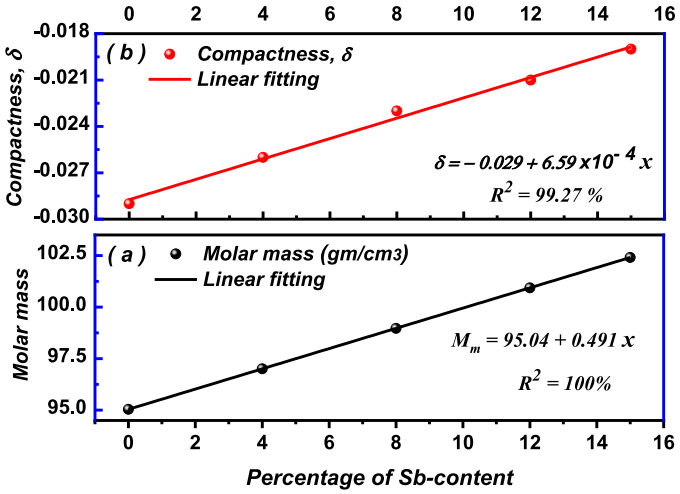

Fig. 3. The dependence of both the molar mass, M_m and the compactness of the sample upon the Sb-content percentage of the chalcogenide $Ge_{15-x}Sb_xSe_{50}Te_{35}$ glasses.

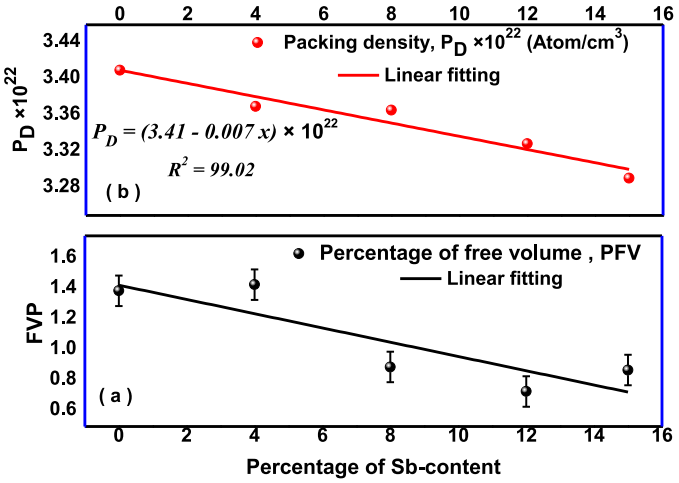

Fig. 4. The change of (a) the percentage of the free volume, FVP and (b) the packing density, P_D of the samples versus the Sb-content percentage of chalcogenide $Ge_{15-x}Sb_xSe_{50}Te_{35}$ glasses.

The estimated values of both V_m and M_m are tabulated in Table 3 and then illustrated in Fig. 2-b and Fig. 3-a, respectively. The variation of both V_m and M_m as a function of the atomic fraction of Sb-content is noted, where the two parameters are linearly increasing with the increase of Sb-content, according to the following empirical equations:

$$V_m = 17.66 + 0.038x \quad (cm^3/mol) \tag{10}$$

and

$$M_m = 95.041 + 0.491x \quad (g/mol) \tag{11}$$

Where x denotes the molar ratio of Sb-element within the bulk composition sample. It is observed that both V_m and M_m show the same behavior as that of the density.

The molar volume is inversely proportional to the density as given in Eq. (2). Thus, it is anticipated that they should follow the opposite trend. However, in the present case of chalcogenide $Ge_{15-x}Sb_xSe_{50}Te_{35}$ bulk glasses, contradictory results are obtained, where both ρ_{Exp} and V_m increase when Sb increases in the system. The rate of change of molar mass is higher than the rate of change of density, which consequently leads to an increase in the molar volume with increasing of antimony within the glassy sample. Similar results are also reported in the previously [4,43]. The found increase in molar volume is also due to the increase in Sb-Se bond length (2.58–2.59 Å) as compared to that of Ge-Se, i.e. (2.36–2.37 Å). This abnormal behavior has already been remarked for several semiconducting materials [4,44,48].

Generally, this anomalous trend supports the concept of open structure [48–50]. Moreover, the theoretically calculated values of the molar volume, V_T of the presently studied chalcogenide samples are also calculated using Eq. (5). The excess volume, V_e is also computed using Eq. (4). The calculated values of both V_T and V_e are also tabulated in Table 3. Depending upon the calculated values of both V_e and V_T, the percentage of free volume, PFV is also estimated from Eq. (6) and is reported in Table 3, and plotted in Fig 4-a as a function of the Sb-concentration. It is found that the theoretical molar volume, V_T, of each sample, is in the good agreement with the experimental values and the difference between these two values is within the value ± 0.13 cm^3/mol.

The compactness, δ-values of the present chalcogenide $Ge_{15-x}Sb_xSe_{50}Te_{35}$ alloys are also calculated and listed in Table 3 and plotted in Fig. 3-b. The values increase from (−0.029) to (−0.019) when the Sb-content increases from 0 to 15%. The graphical representation of this linear relation is fitted to give a straight line, and has the following empirical linear equation:

$$\delta = -0.029 + (6.59 \times 10^{-4}x) \tag{12}$$

Where, x = 0, 4, 8, 12 and 15%, which is the Sb-content percentage. The estimated values of the compactness are negative and increase with Sb addition. The negative and smaller δ-value shows that the chalcogenide $Ge_{15-x}Sb_xSe_{50}Te_{35}$ glassy compositions have an infinitesimal small free volume [3,43,44]. This result is confirmed from the evaluated free volume percentage, FVP, where its values are within one percent (PFV is ranged between 1.39% and 0.89%). Hence, these compositions have small flexibility values [43–45].

On the other hand, the packing density (P_D) is also of importance and is related to the **samples' density**. It can be calculated from Eq. (8). The computed P_D-values are also tabulated in Table 3. Moreover, Fig. 4-b shows the linear relationship between P_D versus Sb-content within $Ge_{15-x}Sb_xSe_{50}Te_{35}$ glassy alloys. The empirical equation that describes the linear representation is given as:

$$P_D = (3.41 - 0.0073x) \times 10^{22} \quad (Atom/cm^3) \tag{13}$$

Where, x is the Sb-content percentage within the chalcogenide $Ge_{15-x}Sb_xSe_{50}Te_{35}$ bulk alloys. It is evident from Table 3 and Fig. 4-b that the packing density decreases from 3.410 × 10^{22} to 3.291 × 10^{22} atom/cm^3 with the subsequent increase in Sb-content from 0% to 15 at.%.

These results are fully consistent with the previous results of M_m and V_m. The found results are very logical, as well as it can be seen that V_m-values are increasing with Sb addition and subsequently result in the decrease of the packing density values, P_D.

Furthermore, these values also imply that the atoms of a certain composition have occupied a larger volume when Sb content increases. This is due to the size of Sb-atom (atomic radius = 161 pm), which is larger than that of the Ge-atom (atomic radius 139 pm). Thereby, the utilized spaces of that composition are increased and consequently results in a decrease in packing density.

3.3. Atomic density and some related parameters

The structural properties of the glass can be illustrated based on the continuous random network model. The atomic density, N_{AD} of an element existing in the chalcogenide $Ge_{15-x}Sb_xSe_{50}Te_{35}$ bulk glasses can be evaluated using Naster–Kingery formula, which is given by the following form [4,51,52];

$$N_{AD} = \frac{\rho_s W_p N_A}{AW \times 100} \tag{14}$$

Where ρ_s is the mass-volume density of the sample, W_P is the percentage of the element in the composition (atomic fraction of the element), N_A

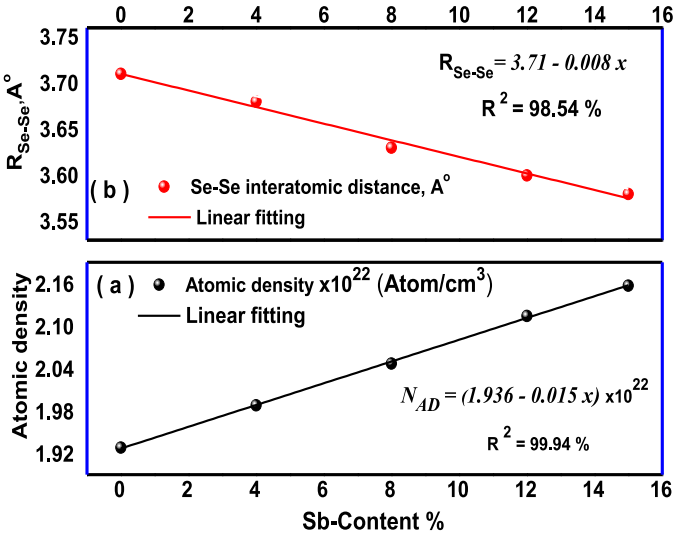

Fig. 5. The variation of both the atomic density, N_{AD} and the Se-Se interatomic separation distance, R_{Se-Se} versus the Sb-content% of chalcogenide $Ge_{15-x}Sb_xSe_{50}Te_{35}$ bulk glassy composition.

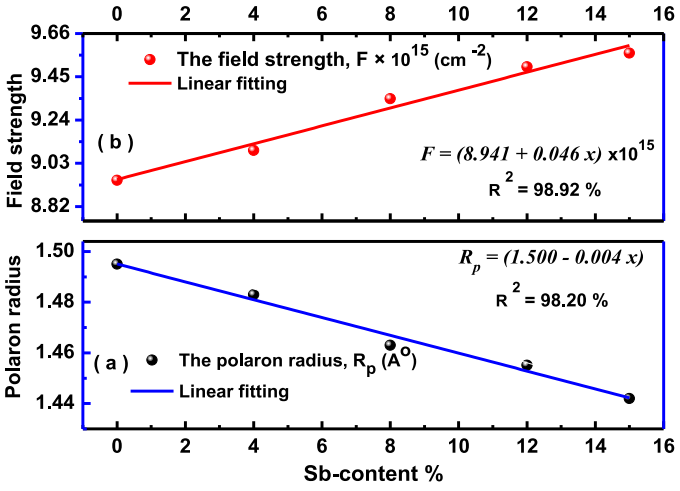

Fig. 6. The linear relationships between both (a) the polaron radius, R_P and (b) the field strength of Se-atom and the Sb-content% of the chalcogenide $Ge_{15-x}Sb_xSe_{50}Te_{35}$ bulk glassy network.

is Avogadro's number, AW is the molar mass ratio of the element content (molar mass of the element divided by the molar mass of its composition) in the glassy Ge-Sb-Se-Te matrix. The atomic density of Sb, Ge and Se are calculated and listed in Table 3, too.

The atomic density of Sb is found to increase from zero to 4.259×10^{21} Atom/cm^3, with the subsequent decrease in the atomic density of Ge, i.e. from 6.361×10^{21} Atom/cm^3 to zero, with the increase of Sb in the host matrix from 0 to 15 at%. The atomic density of Se calculated by employing Eq. (10) is found to increase from 1.962×10^{22} Atom/cm^3 to 2.186×10^{22}Atom/cm^3 when Sb-content increases from 0% to 15%. Fig. 5-a shows the linear dependence of the atomic density of Se upon the percentage of Sb. The empirical equation which describes this dependence is given as follows:

$$N_{AD} = (1.936 - 0.015x) \times 10^{22}(Atom/cm^3) \quad (15)$$

Where, x refers to the ratio of Sb-content%. Fig. 5-a and the above equation shows the decrease of N_{AD}-values with increasing of the percentage of antimony element.

This decrease is presumably due to that the larger atomic size of the Sb-atom as compared to Ge, and consequently results in the decrease in the number of atoms per unit volume with an increase in Sb percent. The interatomic separation between any two neighbours Se-atoms, R_{Se-Se} in the present glassy compositions is estimated from the following simple equation [4,53]:

$$R_{Se-Se} = (1/N)^{1/3} \quad (16)$$

These separation distances have been calculated and reported also in Table 3. They are also represented versus the antimony content in Fig. 5-b. A linear relationship, with a negative slope, between $R_{(Se-Se)}$ and the Sb-content at.% is found, as illustrated in Fig. 5-b, which means that this separation distance decreases as Sb-content increase in the system. This also owing to the atomic size of Sb-element, which is larger than that of Ge-atom, too. This leads to a decrease in this separation distance between any two Se atoms. The equation that characterizes this decrease is given by the following empirical equation:

$$R_{Se-Se} = 3.71 - 0.008x \quad (17)$$

Depending upon the separation distance between every two Se-atoms, the radius of polaron, R_p can be also be determined using the following equations [25,53,54]:

$$R_p = \frac{1}{2}\left(\frac{\pi}{6N}\right)^{1/3} = \left(\frac{\pi}{48N}\right)^{1/3} = 0.403\,R_{Se-Se} \quad (18)$$

Consequently, R_p can be estimated and then recorded in Table 3 and in the same time, it is depicted as a function of Sb-content percent in Fig. 5-a. It is noted that the polaron radius, R_p decreases from 1.495 Å to 1.442 Å when the Sb-content increases, which attributes to the decrease in the interatomic separation between the selenium atoms. The linear proportion between R_{Se-Se} and Sb-content is depicted in Fig. 6-a along with its empirical linear relation can be expressed as:

$$Rp = (1.500 - 0.004x) \quad (Å) \quad (19)$$

The field strength, F is also an important parameter that gives the strength of the Se-field that affects the other atoms located in its surrounding. This parameter is evaluated by knowing the valence number of Selenium, $V_{No.}$ and the polaron radius, R_p as follows [51,52]:

$$F = \left(\frac{V_{No.}}{R_p^2}\right) \quad (20)$$

The values of the field strength are determined and listed in Table 3 and are also shown as a function of Sb-content in Fig. 6-b. This representation gives a straight line of the following empirical equation:

$$F = (8.941 + 0.046x) \times 10^{15}(cm^{-2}) \quad (21)$$

Where, x = 0, 4, 8, 12 and 15 at.%, of the Sb-element presented in the chalcogenide $Ge_{15-x}Sb_xSe_{50}Te_{35}$ alloy. As obvious, the field strength increases as the Sb-content increases. This is attributed to the decrease in the interatomic separation distance between the Se-atoms.

The Fig. 6-a and (b) depict that there is a decrease in the values of polaron radius and an increase in the values of the field strength. This may also be due to the larger size of Sb-atom, where an increase in the atomic size leads to stronger fields.

The comparison of the obtained results of the present investigated parameters of GSST samples, are in good agreement with previously published work [55–58] for similar samples and compounds. S. Mishra and et al. have studied and discussed similar samples of $(Ge_{11.5}Se_{67.5}Te_{12.5})100\text{-}xSbx$, and the current results are in good conformity with their results [55,56].

3.4. Optical studies

3.4.1. Reflectance, R and transmittance, T spectra

Fig. 7-a and b depict the spectral variation of the corrected spectra of the reflectance, R and the transmittance, T, respectively. These figures show that, before the region of the absorption edge, the summation of R% and T% are equal to 100%, approximately i.e. T + R ≈ 100%.

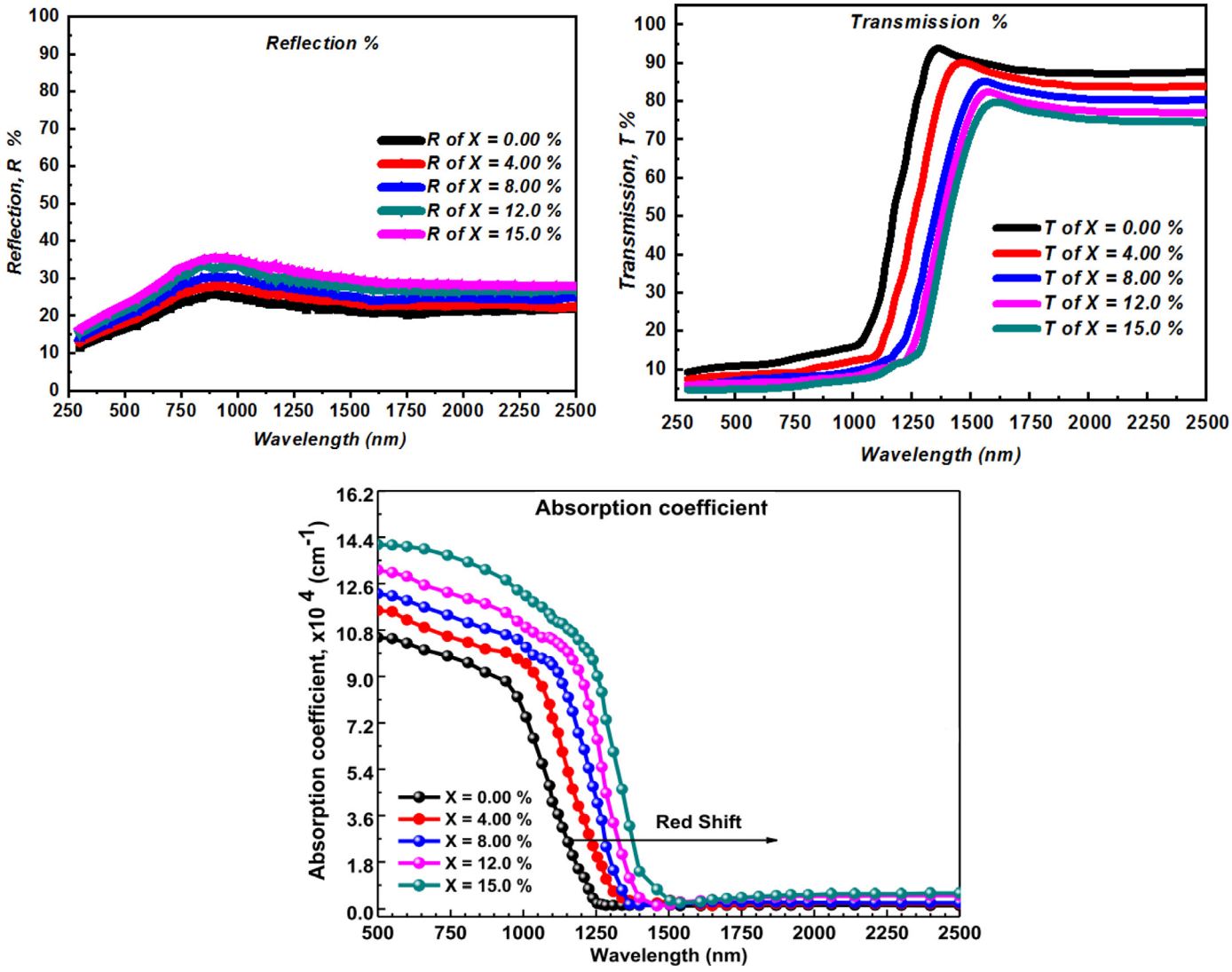

Fig. 7. The spectral dependence of R and T as well as the absorption coefficient (α) with photon wavelength for $Ge_{15-x}Sb_xSe_{50}Te_{35}$ thin films.

This result confirms the smooth surface and good quality of films, where the incident light either transmitted or reflected, there is no scattered or absorbed light. It is noted also that, from the transmittance curves, as illustrated in Fig. 7-b, the absorption edge is shifted towards higher wavelengths when Sb replaced Ge, where it is shifted from about 1000 to 1450 nm. Moreover, the Sb-addition to the expense of Ge causes a reduction in the transmission, while it leads to an increase in the reflectance of films. Furthermore, after the absorption-band edge, and near-infrared region, N-IR all $Ge_{15-x}Sb_xSe_{50}Te_{35}$ films have high transmittance (T ≈ 80%). This transparent nature is decreasing as the Sb-content increases, which is owing to the dark nature of the antimony.

Furthermore, The absorption coefficient spectra **were** computed by employing the corrected values of both the transmittance and the reflectance, using the following Eq. [31,56]:

$$\alpha = \frac{1}{d} \ln \left[\frac{(1-R)^2}{2T} + \sqrt{\frac{(1-R)^4}{4T^2} + R^2} \right] \quad (22)$$

Where d is the film thickness. The variation of **α** upon incident photon wavelength is shown in Fig. 7. Ahead of the band-edge of the absorption, the absorption coefficient (α) has high values ranging between 10^4 and 10^5 cm^{-1}. The found high values of (α) before the band-edge of the absorption are due to the resonance effects which may take place between the photons of the incident light and electrons of the film sample. This resonance between the electrons and phonos leads to restricting the light speed within the film [25]. While, at the higher wavelengths and lower energy values (after a wavelength almost equal to 1450 nm), alpha decreases and approaches to 0. This sudden decrease in α-values at the absorption band-edge of Ge15-xSbxSe50Te35 $Ge_{15-x}Sb_xSe_{50}Te_{35}$ thin films is due to the coupling of the electrons with each other for all samples.

3.4.2. Refractive index

The refractive index, n is a significant physical property of any material. It almost controls the optical and electronic properties of the material. It is also tightly correlated to the electronic polarizability (α_p) of materials' ions and the domestic fields within the material. Therefore, the study of the interrelationship between (n) and (α_p) for any semiconducting material has a great scientific interest, due to the possibility of usage of this semiconducting material in the manifold optoelectronic applications and devices such as the switches, filters and modulators and some other integrated optical devices [59,60]. The refractive index value of the present $Ge_{15-x}Sb_xSe_{50}Te_{35}$ is computed from the spectral measurements of the reflectance (R) and transmittance (T) after their corrections by using a software program. Murmann's exact equations have been used after minimizing $|\Delta T|^2$ and $|\Delta R|^2$ simultaneously as follows [32,47,50]:

$$|\Delta T|^2 = |T_{exp} - T_{cal}|^2 \quad \text{and} \quad |\Delta R|^2 = |R_{exp} - R_{cal}|^2 \tag{23}$$

Where, T_{exp}, T_{cal}, R_{exp} and R_{cal} are values of transmission and reflection (obtained experimentally and theoretically). [32]. It should be noted that the used computer program enables to avoid the restrictions that are used by Murmann's equation [32,50] without any simplifications. In the present study, Murmann's equation solution is dependent on the determination of equal reflection and equal transmission curves crossing".

Hence, the index of refraction is estimated for the amorphous $Ge_{15-x}Sb_xSe_{50}Te_{35}$ film samples from the spectral values of T and R, as follows [32,61–63]:

$$T = \frac{4n}{(n+1)^2} \quad \text{and} \quad R = \frac{(n-1)^2}{(n+1)^2} \tag{24-a}$$

Due to the high values of the absorption coefficient of the present GSST samples, the extinction coefficient also plays a very crucial role in the optical properties of the samples. Therefore, by using Kramers–Kronig relation, R can be reformulated as follows [62–64]:

$$R = \frac{[(n-1)^2 + k^2]}{[(n+1)^2 + k^2]} \tag{24-b}$$

By solving the last equations simultaneously, to get [33,56]:

$$n = \left(\frac{1+R}{1-R}\right) + \left[\frac{4R}{(1-R)^2} - k^2\right]^{1/2} \tag{24-c}$$

The spectral dependence of the refractive index as a function of the incident photon energy for all thin film samples of the present glassy matrix is shown in Fig. 8-a, with varying Sb-concentration percentage. With an increase in antimony, refractive index values are found to increase from 2.834 to 3.109 (in the lowest energy region, till 1.0 eV) when the Sb-content increases, as shown in Fig 8-b. Hence, the value of the refractive index of samples depends upon the stoichiometry of $Ge_{15-x}Sb_xSe_{50}Te_{35}$ glassy matrix. Also, as discussed in previous work [32], the increase in average cross-linking density with Sb addition also accounts for this increase in n values. These estimated values are in good agreement with S. Mishra and et.al. [56]. This increase in n values is also attributed to the high polarizability values due to larger Sb [65], in addition to the increase in density values as discussed above.

3.4.3. Electronic polarizability

The average electronic polarizability of ions is studied because it is one of the unique features of any material and many optoelectronic applications are based on it. On exposure of an intense electric field, the polarization does not remain proportional to the electric field, but instead, becomes dependent on the square of electric field and cause non-linearity. Thus the electronic polarizability also governs the nonlinear response of the material [66,67]. Therefore, from the application point of view, the materials with high optical non-linearity can be designed. Many linear optical properties have been correlated with the electronic polarizability, based on the relation given by many workers [25,66–68]. This study of polarizability also provides an understanding of the relationship between covalent/ionic nature of bonds and other optical parameters. The current class of chalcogenide $Ge_{15-x}Sb_xSe_{50}Te_{35}$ matrix shows a dependence of refractive index on the intensity of an incident photon. Therefore, the study of their polarizability is an essential issue.

3.4.3.1. Molar refractivity and polarizability:. The molar refractivity, R_m is a measure of the total polarizability of one mole of a substance. It depends upon the refractive index and for amorphous material, it is given by the Lorentz-Lorentz equation. Therefore, for the investigated material, R_m is given as [25]:

$$R_m = \frac{(n^2-1)}{(n^2+2)}\frac{M}{\rho} \quad \text{or} \quad R_m = \frac{(n^2-1)}{(n^2+2)}V_m, \tag{25}$$

Where, $V_m = \frac{M}{\rho}$ is the molar volume and n is the refractive index. According to, Clausius–Mosotti relation, electronic polarizability is related to the average molar refraction and is given by the following relationship [25]:

$$R_m = \frac{4\pi N}{3}\alpha_p \text{or} \alpha_p = \frac{3R_m}{4\pi N} \tag{26}$$

Where α_p is the magnitude of the electric response by the electron clouds when an electromagnetic wave is incident on thin films and N is the Avogadro's number. Consequently, using the Lorentz-Lorentz equation, the molar refractivity value can be calculated for all the samples under investigation and then its values are also tabulated in Table 4 for all the Sb-concentrations. An increase in R_m values are found in $Ge_{15-x}Sb_xSe_{50}Te_{35}$ glassy matrix and follows the given empirical relationship with Sb-content.

$$R_m = 12.34 + 0.076\,x \tag{27}$$

From Clausius–Mosotti relation and calculated values of molar refractivity, from Lorentz-Lorentz equation [25], the electronic polarizability is also calculated (Table 4). The tabulated polarizability behavior shows an increase in the obtained values from 4.91 to 5.39, with an addition of more Sb-content in the matrix and also linearly fitted as shown in Fig. 7, to get this empirical equation:

$$\alpha = 1.41\ n + 0.98 \tag{28}$$

On the other hand, using the values of bulk modulus, the optical electronegativity and the optical band gap energy in Clausius–Mossotti

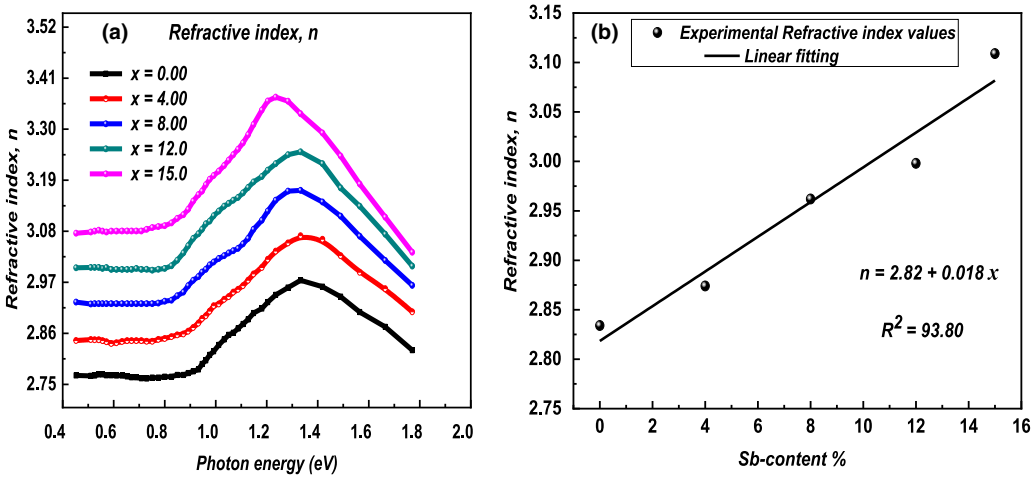

Fig. 8. Illustration of the refractive index, *n* as (a) spectra *Vs* the photon energy and (b) its variation with the Sb-content present.

Table 4
Some other evaluated parameters of a-$Ge_{15-x}Sb_xSe_{50}Te_{35}$ bulk and thin film samples.

The evaluated Parameter	Quaternary chalcogenide $Ge_{15-x}Sb_xSe_{50}Te_{35}$ bulk glasses				
	x = Zero	x = 4	x = 8	x = 12	x = 15
Experimental n-values [32]	2.834	2.874	2.962	2.998	3.109
Molar refractivity	12.38	12.64	12.91	13.15	13.59
Electronic polarizability in Å^3 using Eq. (29)	4.91	5.01	5.12	5.21	5.39
Electronic polarizability in Å^3 using Eq. (31)	5.74	5.85	5.924	6.018	6.119
Reflection loss,	0.701	0.707	0.721	0.726	0.742
Covalence parameter	0.306	0.292	0.278	0.273	0.251
Optical electronegativity	1.732	1.726	1.712	1.708	1.69
Indirect band-gap energy, Eg (eV) [31,32]	1.047	0.987	0.928	0.898	0.864
Average heat of atomization, HS (kCal/g.atom)	54.300	53.180	52.060	50.940	50.100
Optical energy gap, Eg (eV) [31,32]	1.047	0.987	0.928	0.898	0.864
Deviation from stoichiometry, R	2.833	3.036	3.269	3.542	3.778
Overall mean bond energy, <E> (eV)	2.42	2.29	2.21	2.13	2.07
Glass Transition temperature Tg (K)	472.72	432.29	407.41	381.90	362.62

relation, the electronic Polarizability values in Å^3 (Table 4) are also calculated as follows [58]:

$$\alpha = 0.395\left(\frac{12.41 - \sqrt{Eg - 0.365}}{12.41 + 2\sqrt{Eg - 0.365}}\right)\left(\frac{M}{\rho}\right) \quad (29)$$

Where E_g, M and ρ are the optical band gap energy, molecular weight value and density of the material of the sample, respectively.

The optical electronegativity difference Δχ is taken from Dufy's equation [54] by the substitution of band gap values, i.e. $\Delta\chi = 0.2688\ E_g$. The band gap energy values are already calculated and communicated in previous work [31,32]. Bulk modulus can also be calculated based on electronegativity using given relation [69,70]:

$$B = 168.58 + 30.3\ \ln(0.102\ \Delta\chi) \quad (30)$$

Therefore, Clausius-Mossotti relation in term of the bulk modulus, the electronic polarizability is given as:

$$\alpha = 0.395\left(\frac{(5.563 - 0.033\ B)^2 - 1}{(5.563 - 0.033\ B)^2 + 2}\right)\left(\frac{M}{\rho}\right) \quad (31)$$

After rearranging in term of k, where: $k = (\ln \Delta\chi)(\ln \Delta\chi - 4.464)$. Besides, in term of the optical band gap energy, the electronic polarizability is given by Eq. (29).

A subsequent increase in polarizability values (calculated using both relations) has been noted down with the increase in Sb content. This polarizability follows the following empirical relationship with refractive index values (best fitting from Fig 9):

$$\alpha = 1.088\ \ n + 2.74 \quad (32)$$

This increase is attributed to the larger radius value of Sb (1.38 Å) as compared to Ge (1.22 Å). By following the Lorentz–Lorenz relationship, it is evident that a greater atomic radius helps in achieving greater polarizability (α_{pi}) and consequently results in higher values of the refractive index [73,74]:

$$\frac{n^2 - 1}{n^2 + 2} = \frac{1}{3\varepsilon_o}\sum_i N_i\alpha_{pi} \quad (33)$$

Where, N_i the number of polarizable units per unit volume, and ε_0 is the vacuum permittivity. Moreover, the density of Sb (6.69 g/cc at 20 °C) is also larger than that of Ge (5.32 g/cc at 20 °C), which is also one of the factors of this found an increase in polarizability and leading the system towards higher refractive index values. Density values are already calculated (mentioned earlier) and refractive index values are also making a direct relationship with these values (shown earlier). This further leads towards the increase in the volume of electronic spaces [63,71,72]. This observed increase in the polarizability value also indicates the increase in the mobility of electrons in the glassy system,

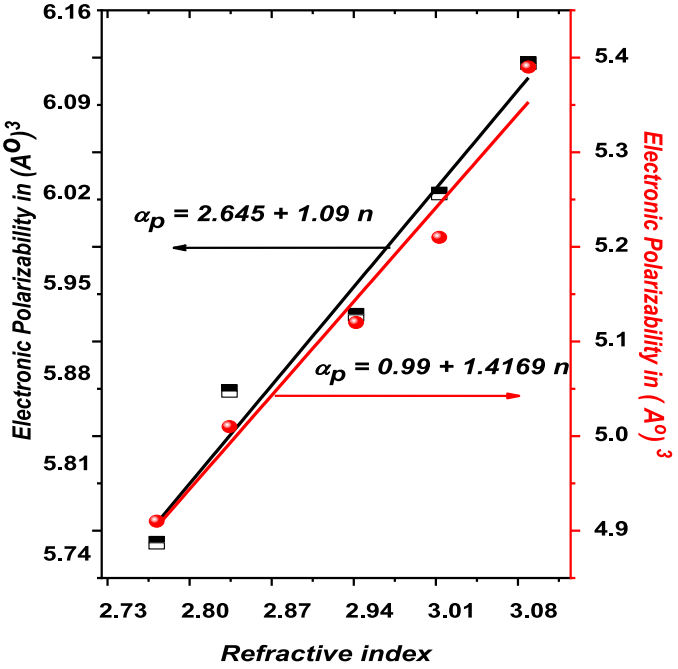

Fig 9. The interrelationships between the electronic polarizability and the refractive index.

which further accounts for the rise in molar reflectivity, as discussed above, and the refractive index values.

3.4.3.2. Reflection loss. Using the experimentally obtained values of refractive index, the reflection loss can be also calculated, as given by [25]:

$$RL = \frac{n^2 - 1}{n^2 + 2} \quad (34)$$

The calculated values of RL are also tabulated in Table 4 and show an increase with increasing Sb in the system. Increasing values of extinction coefficient (in previously published work) also show an increase in absorption and scattering losses with Sb addition. The variation of RL with Sb content is shown in Fig. 10-a and found to follow this given empirical relationship:

$$RL = 0.699 + \ 0.0026\ x \quad (35)$$

This increase in RL and R_m values subsequently accounts for the found increase in polarizability. Moreover, a linear relationship found between refractive index and polarizability also confirms the

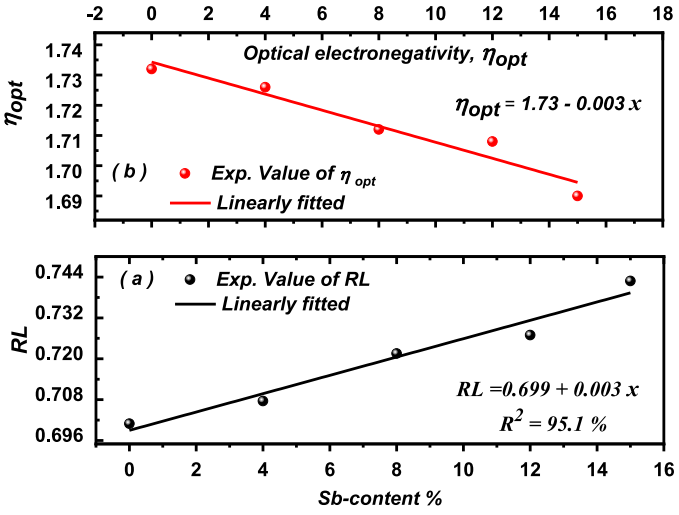

Fig 10. Variation of both (a) Reflection loss and (b) optical electronegativity versus Sb-content at.% of Ge-Sb-Se-Te film samples.

amorphous nature of the films as suggested by Zemel J.N. et al. Therefore, this result is in good consistency with what argued by Zemel J.N. et al. [75].

3.4.4. Covalence parameter and optical electronegativity

The covalence parameter defines the metallic or insulation characteristic of the investigation samples. It is also known as metallization parameter or metallization criteria, denoted by M and is given by [25]:

$$M = 1 - (R_m/V_m) = 1 - RL, \quad (36)$$

Where *Rm* is the average molar refraction and *Vm* is the molar volume. $M > 1$ depicts the metallic character of the materials. On the other hand, insulating behavior is shown with $M < 1$. The calculated covalence values are tabulated in Table 4 for $Ge_{15-x}Sb_xSe_{50}Te_{35}$ glassy matrix. The M values are less than 0.300, i.e. $M << 1$, for all the samples. Therefore, thin films of Ge-Sb-Se-Te are not metallic. It is observed that with the increase in Sb, covalence parameter shows a decrease from 0.29 to 0.25, i.e. matrix is tending towards the metallic character. This decrease in metallization parameter also accounts for the reduction in the optical band gap [31,32] found in material with an increase in Sb in the system. Therefore, dropping in the of *M*-values hints towards the decrease in the forbidden gap as well as the widening of the conduction band in the energy level, which makes the system more conductive.

According to Duffy [76,77], many physical-chemical parameters of the materials can be assessed using notions of optical electronegativity and is given by [25,67]:

$$\eta opt = (A/n)^{1/4}, \quad (37)$$

Where $A = 25.54$ and is a unitless constant [63,77], and *n* is the refractive index. Optical electronegativity defines the tendency of an atom or radical to attract electrons and to form the ionic bond. The Duffy model is applicable to the materials mostly used in optoelectronic industry [76]. Hence, it can be applied in the present investigating system. The calculated values of optical electronegativity are listed in Table 4 and plotted also against Sb-content, as depicted in Fig. 10-b. An inverse linear relationship is obtained and follows the given empirical relationship.

$$\eta opt = 1.73 - 0.003\,x \quad (38)$$

Optical electronegativity also hints towards the nature of the bonding in the materials. The values are found to decrease with an increase in Sb in the system. This decrease is due to its inverse relationship with the refractive index. The small changes in the electronegativity values can also be due to the covalent nature of the system. These results are consistent with the other previous literature [57,58].

3.5. Determination of average heat of atomization H_s

The average heat of atomization, H_s is defined as the energy needed to take apart only one mole of a certain material into its atoms. It is also given as the quantity of energy that is needed to transform a suitable quantity of an element presented in the standard state to one mole of atoms in the gaseous form. The average heat of atomization of the bulk quaternary chalcogenide composition, $A_\alpha B_\beta C_\gamma D_\delta$ can be calculated from the following equation [55,58,78,79]:

$$H_s = \frac{(\alpha H_S^A + \beta H_S^B + \gamma H_S^C + \delta H_S^D)}{(\alpha + \beta + \gamma + \delta)} \quad (39)$$

Therefore, for the present bulk chalcogenide $Ge_{15-x}Sb_xSe_{35}Te_{50}$ glassy matrix, the average heat of atomization is given as follows:

$$H_s = \frac{(\alpha H_S^{Ge} + \beta H_S^{Sb} + \gamma H_S^{Se} + \delta H_S^{Te})}{(\alpha + \beta + \gamma + \delta)} \quad (40)$$

Consequently, H_s of the studied $Ge_{15-x}Sb_xSe_{35}Te_{50}$ glassy network can be calculated by knowing the heat of atomization constituent elements given in Table 1. The estimated H_s-values of the present study samples GSST are given in Table 4 and plotted in Fig. 11-b. The value of $\mathbf{H_s}$ is in a linear relationship with Sb-content%. The empirical equation that describes the inversely proportional relation between H_s and Sb-content is given as follows:

$$H_S = 54.3 - 0.28\,x \quad (41)$$

Where, x represents the percentage of Sb-content. The average heat of atomization decreases as the Sb-content is increased. This is because the heat of atomization of Sb-element is less than that of Ge-element (H_s of Sb = 62 kCal/g.atom, while for Ge, it is 90 kCal/g.atom). This decrease in H_s is also owing to the decrease of both the band-gap energy, as shown in Fig. 11-a, and the cohesive energy [55,58,83].

3.6. Determination of deviation from stoichiometry, R

The deviation from stoichiometry, *R* can be stated as the ratio of the probable covalent bonds of chalcogen atom to the non-chalcogen atoms. Hence, it defines the deviance from stoichiometry. For the present chalcogenide $Ge_\alpha Sb_\beta Se_\gamma Te_\delta$ glassy matrix, its value is given as:

$$R = \frac{\gamma\langle ECN\rangle(Se) + \delta\langle ECN\rangle(Te)}{\alpha\langle ECN\rangle(Ge) + \beta\langle ECN\rangle(Sb)} \quad (42)$$

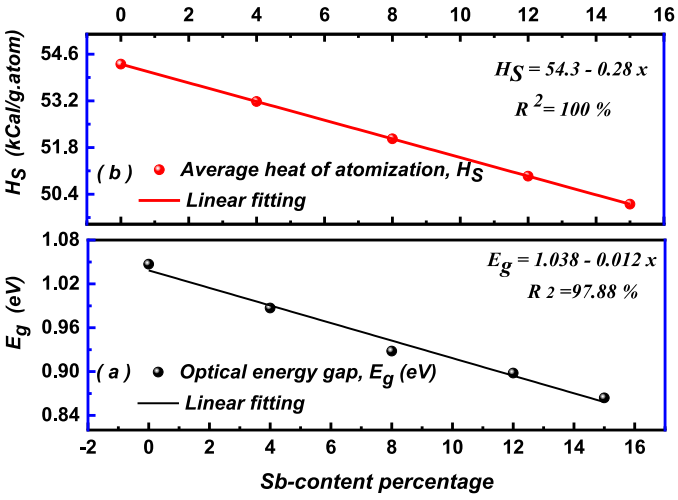

Fig. 11. The linear dependence of the both (a) Energy band gap, E_g and (b) Average heat of atomization, H_s and the Sb-content% of the chalcogenide $Ge_{15-x}Sb_xSe_{50}Te_{35}$ bulk glasses.

Where, α, β, γ and δ are the corresponding atomic fractions of Ge, Sb, Se and Te, respectively and $\langle ECN \rangle$ is the elemental coordination number of each element, i.e. of Ge, Sb, Se and Te [19,80,81]. When R-value is found to be greater than 1, it designates a chalcogen-rich material, containing both heteropolar and 'chalcogen-chalcogen' bonds. But, $R < 1$, infers a chalcogens poor composition, consisting of heteropolar and metal-metal bonds. While, the case of $R = 1$ suggests a stoichiometric composition containing only heteropolar bonds. It mainly shows the minimum chalcogenide content at which chemically ordered network is formed [80,81].

The deviation of stoichiometry for the present investigated $Ge_{15-x}Sb_xSe_{50}Te_{35}$ system is summarized in Table 4. It is observed that for all the studied compositions, R-values are greater than the unity which further hints towards the chalcogens rich material containing heteropolar (i.e. Se-Ge and Se-Sb) and chalcogen-chalcogen (Se-Te) bonds. No sign of chalcogens poor region is seen in this study, as the minimum R-value is 2.83 for the chalcogenide bulk $Ge_{15}Se_{35}Te_{50}$ composition.

3.7. Overall mean bond energy

The mean bond energy is strongly dependent on the cohesive forces or the rigidity of the network. Assuming the chemical bond ordering model, based on a theory developed by Tichy, it can be given as [54,80–85]:

$$\langle E \rangle = \bar{E}_c + \bar{E}_{rm} \tag{43}$$

Where, $\bar{E}_c$ is "the average energy of cross-linking per atom" or the total contribution towards the bond arising from heteropolar bonds. While, $\bar{E}_{rm}$ is referring to the contribution arising from weaker bonds (remaining bonds after the saturation of strong bonds). It describes the "average bond energy per atom" of the residual matrix. Furthermore, the values of E_c and E_{rm} are dependent upon the deviation from stoichiometry, R. It is clear from Table 4 that R values for the present matrix are greater than unity. Therefore, for $R > 1$ [80–83]:

$$\overline{E_c} = P_r E_{hb} \tag{44}$$

Where, E_{hb} is the average heteropolar bond energy of the chalcogenide $Ge_\alpha Sb_\beta Se_\gamma Te_\delta$ glassy system. It can be determined from this equation:

$$E_{hb} = \frac{\alpha\langle ECN\rangle(Ge)E_{Ge-Se} + \gamma\langle ECN\rangle(Sb)E_{Se-Sb} + \delta\langle ECN\rangle(Te)E_{Se-Te}}{\alpha\langle ECN\rangle(Ge) + \gamma\langle ECN\rangle(Sb) + \delta\langle ECN\rangle(Te)} \tag{45}$$

Where, The energies E_{Ge-Se}, E_{Se-Sb} and E_{Se-Te} are energy values of the heteropolar bonds of Ge-Se, Se-Sb and Se-Te bonds, respectively. On the other hand, the degrees of cross-linking per atom (P_r) for $R > 1$ are given by [19,80]:

$$P_r = \frac{\alpha\langle r\rangle(Ge) + \gamma\langle r\rangle(Sb) + \delta\langle r\rangle(Te)}{\alpha + \beta + \gamma + \delta} \tag{46}$$

While, for $R > 1$, too, $\overline{E_{rm}}$ is given by this equation:

$$E_{rm} = \frac{2(0.5 < r > - P_r)}{<r>} E_{Se-Se} \tag{47}$$

The calculated values of the mean bond energy are also tabulated in Table 4 and shown in Fig. 12-a as a function of Sb-content. It is found that the mean bond energy decreases linearly with an increase in Sb content, according to this empirical equation:

$$< E > (eV/bond) = 2.401 - 0.022x \tag{48}$$

Where, x is the Sb-percentage in the $Ge_{15-x}Sb_xSe_{50}Te_{35}$ glassy composition. $< E >$ depends on the bond energy values of the system, therefore it also follows the same trend as that of cohesive energy and the band gap of the system. Comparable results are also reported for other chalcogenide networks [19,43,44].

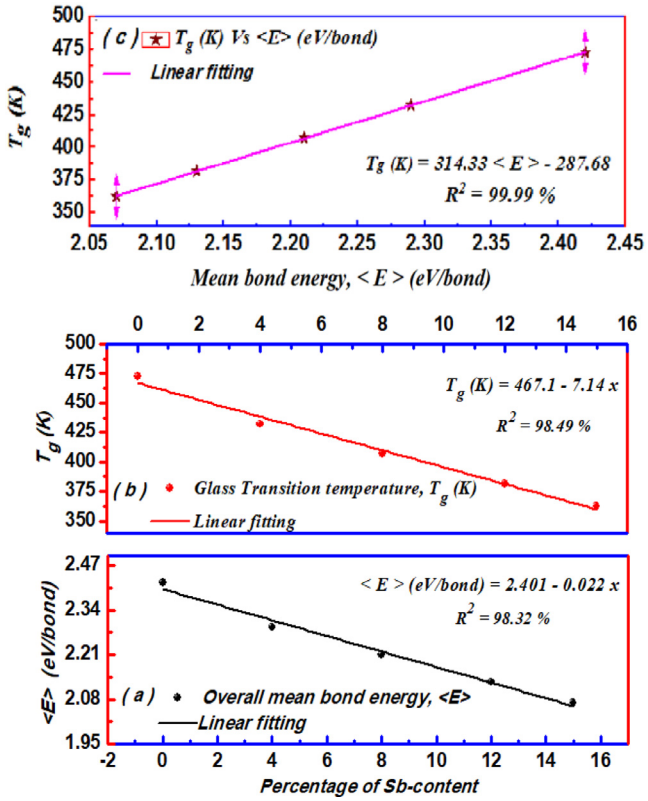

Fig. 12. The linear proportionality between both (a) The overall mean bond energy, $<E>$ and (b) The Glass Transition temperature, T_g (K) and the Sb-percentage, in addition (c) The linear relationship between T_g (K) and $<E>$ of the $Ge_{15-x}Sb_xSe_{50}Te_{35}$ bulk glassy matrix.

3.8. Glass transition temperature, T_g

The glass transition temperature is the temperature beyond which the amorphous composition can achieve numerous structural arrangements, while below which this amorphous retains its structural form. Above T_g, the viscosity of the system presumably drops down due to the breakdown of the glassy network. Therefore, a correlation between T_g and network rigidity is also expected. The value of this temperature is also in a direct relationship with the energy that is required to break the covalent bonds of the non-crystalline systems and re-form them again. In the chemically ordered system, according to Thorpe, Tichy and Ticha [82,84]. The values of T_g are not only related to the network structure, but besides this also holds an excellent empirical correlation with mean bond energy $\langle E \rangle$ of the system. A chemical order network is expected in an investigated system, considering the substantial difference in the bonding energies of heteropolar bonds from homopolar bonds. Tichy and Ticha examined approximately 200 sets of binary and ternary glasses and obtained a correlation of glass transition temperature with mean bond energy.

Based on the determined values of $< E >$, T_g is calculated by using the following emperical form [4,43,80]:

$$T_g = 311(<E> - 0.9) \tag{49}$$

Hence, using the estimated $< E >$ values, T_g-values are evaluated and tabulated in Table 4 and shown as a function of the Sb-percentage in Fig. 12-b. With an increase in Sb in the system, mean bond energy $\langle E \rangle$ and Glass transition temperature T_g values are found to decrease as per the following empirical formulas:

$$< E > (eV) = 2.401 - 0.02\,x \tag{50}$$

And,

$$T_g(K) = 467.06 - 7.14\ x \quad (51)$$

Where, x is the Sb-content percentage within the glassy $Ge_{15-x}Sb_xSe_{50}Te_{35}$ system. Due to the weak Van der Waal interactions, the covalent bonding is dominant in glassy materials and therefore, cohesive energy also corresponds to bond energy.

Furthermore, the glass transition temperature, E_g is linearly increases with increase in the mean bond energy for the present matrix, as shown in Fig. 12-c according to this empirical form:

$$Tg(K) = 314.23 < E > -287.68 \quad (52)$$

Where, <E> is the mean bond energy of the present Ge-Sb-Se-Te matrix expressed in (eV/bond). This increasing in E_g-values is attributed to the aggregation of the structural units of Se-Ge, Se-Te and Se-Sb in the three dimensions [79,84,85]. Similar results are reported in the literature for many similar chalcogenides [4,19,43,44,80].

Consequently, T_g is linked linearly also with the magnitude of the cohesive forces within the glassy network. The glassy matrix of $Ge_{15}Se_{50}Te_{35}$ shows the point of the existence of a majority of heteropolar bonds, and chemical bond energies are maximized at this and this has subsequently been one of the reasons for the high value of glass transition temperature at these compositions. But this model does not provide any information about the molecular interactions, and these interactions have a major role in the relaxation process in the glassy region [82-84].

According to the mechanical point of view, glasses, the microhardness of a material is an experimentally accessible parameter. Therefore, it should be related to mean bond energy or bond strength. Hence, after studying about 190 sets of chalcogenide glasses, Ruben and his associates [38,85] gave an empirical relation between T_g (K) and H (kg/mm^2) as follows:

$$T_g = 1.6H + 211 \quad (53)$$

This shows a linear dependence of the microhardness of the present glassy alloys on the glass transition temperature, T_g and mean bond energy $<E>$. Therefore, it is clear that with the subsequent decrease in mean bond energy and glass transition temperature, the microhardness of the investigating system is also decreasing.

4. Conclusions

Bulk samples of the quaternary chalcogenide Ge_{15-x} Sb_x Se_{50} Te_{35} are synthesized via melt quench technique. XRD spectra show an amorphous nature of GSST glassy alloys owing to the absence of any sharp peak in the X-ray patterns. The physical properties of $Ge_{15-x}Sb_xSe_{50}Te_{35}$ glassy matrix are studied and discussed. Density values, molar volume, molar mass, atomic density, field strength, number of valence electrons, are found to increase with the substitution of Ge by Sb in the Ge-Sb-Se-Te host matrix. On the other hand, excess volume, free volume percentage, compactness, packing density, interatomic separation distance, polaron radius are found to decrease with the Sb addition. An increase in electronic polarizability accounts for the increase in the refractive index of the glassy matrix. Covalence parameter shows $M > 1$, for all the compositions, hints metallic character in the samples. This means the system is chalcogens rich and an open structure is expected in it. The drop in the covalence parameter values hints towards the decrease in band gap energy and broadening of the conduction band. Optical electronegativity values are found to decrease with an increase in Sb content. Along with, the deviation from stoichiometry, average heat of atomization, overall mean bond energy and the glass transition temperature have been also evaluated and discussed. It is found that the deviation from the stoichiometry values are greater than the unity for the study samples of GSST matrix and at the same time increases which further hints towards the chalcogens rich material containing heteropolar bonds. On the other hand, the values of the average heat of atomization, overall mean bond energy and the glass transition temperature decreases as Sb-content is increased. Changes in the network of the glassy matrix affect the physical parameters of each composition. The present study recommends that Ge-Sb-Se-Te samples can be employed in several nonlinear optical applications and devices. Where, the physical and optical parameters of the Ge_{15-x} Sb_x Se_{50} Te_{35} samples can be tuned and engineered as per requirements.

Funding

This research was not funded by any authority, the authors bear all the costs of the work.

CRediT authorship contribution statement

Ahmed Saeed Hassanien: Conceptualization, Data curation, Formal analysis, Investigation, Methodology, Project administration, Resources, Software, Supervision, Validation, Visualization, Writing - original draft, Writing - review & editing. **Ishu Sharma:** Conceptualization, Data curation, Formal analysis, Investigation, Methodology, Project administration, Resources, Software, Supervision, Validation, Visualization, Writing - original draft, Writing - review & editing. **Alaa A. Akl:** Conceptualization, Data curation, Formal analysis, Investigation, Methodology, Project administration, Resources, Software, Supervision, Validation, Visualization, Writing - original draft, Writing - review & editing.

Declaration of Competing Interest

The authors declare that they have no conflict of interest.

References

[1] J.H. Lee, J.H. Choi, J.H. Yi, W.H. Lee, E.S. Lee, Y.G. Choi, Sci. Rep. 8 (2018) 15482.
[2] Kadonok, J. Ceram. Soc. Jpn. 115 (5) (2007) 297.
[3] J. HoLee, W.Lee J.Yi, B. JePark, Y. Gyu Choi, J. Non-Cryst. Solids 481 (2018) 21–26.
[4] A.S. Hassanien, A.A. Akl, J. Non-Cryst. Solids 428 (2015) 112–120.
[5] D. Vipin Kumar, K. Dwivedi, Optik 124 (2013) 2345.
[6] A.S. Hassanien, A.A. Akl, J. Non-Cryst. Solids 432 (2016) 471–479.
[7] A.S. Hassanien, A.A. Akl, Superlattices Microstruct. 89 (2016) 153–169.
[8] I. Sharma, S.K. Tripathi, P.B. Barman, J. Appl. Phys. 110 (2011) 043108-7.
[9] J. Eggleton, B. Luther-Davies, K. Richardson, Nat. Photonics 5 (2011) 141.
[10] J.K. Behera, X. Zhou, J. Tominaga, R.E. Simpson, Opt. Mater. Express 7 (2017) 3741–3759.
[11] G.-H. Jung, H. Kong, J.-B. Yeo, H.-Y. Lee, J. Korean Ceramic Soc. 54 (6) (2017) 484–491.
[12] A.S. Hassanien, A.A. Akl, CrystEngComm 20 (2018) 7120–7129.
[13] F. Désévédavy, G. Renversez, J. Troles, P. Houizot, L. Brilland, I. Vasilief, Q. Coulombier, N. Traynor, F. Smektala, J.L. Adam, Opt. Mater. 32 (2010) 1532.
[14] S.A. Fayek, M. El-Ocker, A.S. Hassanien, Mater. Chem. Phys. 70 (2001) 231–235.
[15] S. Mishraa, P. Lohia, D.K. Dwivedi, Infrared Phys. Technol. 100 (2019) 109–116.
[16] I. Sharma, P. Kumar, S.K. Tripathi, Phase Transitions 90 (7) (2017) 653–671.
[17] G. Abbady, A.M. Abd-Elnaiem, Phase Transitions 92 (7) (2019) 667–682.
[18] N.F. Mott, E.A. Davis. second ed.Oxford: Clarendon Press, (1979).
[19] P. Vashist, B.R. Singh Patial, Anjali, Nagesh Thakur, AIP Conference Proceedings 1953, 2018090085.
[20] P. Bavaf, M. Rezvani, Results Phys. 10 (2018) 777–783.
[21] I. Sharma, A. Kumar, S.K. Tripathi, P.B. Barman, J. Phys. D 41 (17) (2008) 175504–175508.
[22] R. Chauhan, A.K. Srivastava, M. Mishra, K.K. S.rivastava, Integr. Ferroelectr. 117 (2010) 22.
[23] K. Shimakawa K, J. NonCryst. Solids 77/78 (2) (1985) 1253.
[24] A.S. Hassanien, A.A. Akl, J. Non-Cryst. Solids 487 (2018) 28–36.
[25] A.S. Hassanien, J. Alloys Compd. 671 (2016) 566–578.
[26] M.M. El-Ocker, S.A. Fayek, F. Metawe, A.S. Hassanien, Indian J. Phys. A 72 (1998) 31–42.
[27] A.S. Hassanien, K.A. Aly, A.A. Akl, J. Alloys Compd. 685 (2016) 733–742.
[28] A.S. Hassanien, A.A. Akl, Superlattices Microstruct. 85 (2015) 67–81.
[29] P. Kumar, J. Kaur, S.K. Tripathi, I. Sharma, Indian J. Phys.91 (12), 1503–1511.
[30] P. kumar, S.K. tripathi, I. sharma, J. Alloys Compd. 755 (2018) 108–113.
[31] A.S. Hassanien, I. Sharma, J. Alloys Compd. 798 (2019) 750–763.
[32] A.S. Hassanien, I. Sharma, Optik 200 (2020) 163415 https://doi.org/10.1016/j.ijleo.2019.163415.
[33] B. Chen, G. Chen, W. Wang, H. Cai, L. Yao, S. Chen, Sol. Energy 176 (2018) 98–103.

[34] S.S. Fouad, G.A.M. Amin, M.S. El-Bana, J. Non-Cryst. Solids 481 (2018) 314–320.
[35] S. Yoo, C. Yoo, E. Park, W. Kim, Y. Lee, C. Hwang, J. Mater. Chem. C 6 (2018) 5025–5032.
[36] CRC Handbook of Chemistry and Physics, editor, in: David R. Lide (Ed.), CRC Handbook of Chemistry and Physics, 88th edition, Taylor & Francis Group, Boca Raton, Florida, 2008.
[37] L. Pauling, The Nature of the Chemical Bond, 3rd edition, Cornell University Press, Ithaca, NY, 1960.
[38] Handbook of the Elements, Samuel Ruben January 8, Open Court Publishing Company, La Salle, Illinois, 1999, p. 61301.
[39] A.S. Hassanien, A.A. Akl, Appl. Phys. A 124 (2018) 752.
[40] A.S. Hassanien, A.A. Akl, A.H. Sáaedi, Cryst. Eng. Comm. 20 (2018) 1716–1730.
[41] A.A. Akl, S.A. Mahmoud, S.M. AL-Shomar, A.S. Hassanien, Mater. Sci. Semicond. Process. 74 (2018) 183–192.
[42] I. Sharma, A.Z. Khan, J. Optoelectron. Adv. Mater. 19 (11–12), 778–787.
[43] A. Dahshan, K.A. Aly, J. Non-Cryst. Solids 408 (2015) 62–65.
[44] I. Sharma, S. Sunder, Mater. Sci.-Pol. 36 (2) (2018) 242–254.
[45] S. Sharda, N. Sharma, P. Sharma, V. Sharma, J. Non-Cryst. Solids 362 (2013) 136–139.
[46] M. Vlc˘ek, M. Frumar, J. Non-Cryst. Solids 97 (1987) 1223.
[47] V. Pamukchieva, A. Szekeres, M. Todorova, E. Svab, Z.S. Revay, L. Szentmiklosi, J. Non-Cryst. Solids 355 (2009) 2485.
[48] M. Farouk, A. Samir, F. Metawe, M. El-okr, J. Non-Cryst. Solids 371–372 (2013) 14–21.
[49] S. Rada, A. Dehelean, E. Culea, J. Non-Cryst. Solids 357 (2011) 3070.
[50] R.E. Mallawany, M.D. Abdalla, I.A. Ahmed, J. Mater. Chem. Phys. 109 (2008) 291.
[51] H.H. Naster, W.D. Kingery, Proceedings of the Seventh International Conference on Glass, Brussels, Gordon and Breach, New York, 1965, p. 106.
[52] A. Maged, L. Wahab, I. El Kholy, J. Mater. Sci. 33 (1998) 3331.
[53] M. Farouk, A. Samir, M. El Okr, Physica B 530 (2018) 43–48.
[54] C. Bootjomchai, Radiat. Phys. Chem. 110 (2015) 96.
[55] S. Mishra, P. Lohia, D.K. Dwivedi, Physica B 572 (2019) 81–87.
[56] S. Mishra, P. Lohia, D.K. Dwivedi, Infrared Phys. Technol. 100 (2019) 109–116.
[57] E.R. Shaaban, M.Y. Hassaan, M.G. Moustafa, A. Qasem, G.A.M. Ali, E.S. Yousef, Optik 186 (2019) 275–287.
[58] I. Sharma, S.R. Madara, P. Sharma, Materials Today: Proceedings, https://doi.org/10.1016/j.matpr.2019.10.023.
[59] S. Ahmad, M. Mohib-ul Haq, Iran. J. Phys. Res. 14 (3) (2014) 89–93.
[60] R.R. Reddy, S. Anjaneyulu, T.V.R. Rao, Infrared Phys. 33 (5) (1992) 389–393.
[61] S.A. Mahmoud, A.A. Akl, S.M. Al-Shomar, Physica B 404 (2009) 2151.
[62] A.S. Hassanien, A.A. Akl, J. Alloys Compd. 648 (2015) 280–290.
[63] O.S. Heavens, Optical Properties of Thin Solid Films, Dover, New York, 1965.
[64] A.S. Hassanien, A.A. Akl, Physica B 576 (2020) 411718.
[65] E. Marquez, J.M. Gonzalez-Leal, A.M. Bernal-Oliva, R. Jimenez-Garay, T. Wagner, J.Non-Cryst. Solids 354 (2008) 503.
[66] M. Abdel Rafea, A.A.M. Farag, N. Roushdy, J. Alloys Compd. 485 (2009) 660.
[67] M.N. Azlan, M.K. Halimah, S.Z. Shafinas, W.M. Daud, Mater. Express 5 (3) (2015) 211.
[68] V. Dimitrov, S. Sakka, J. Appl. Phys. 79 (1996) 1736.
[69] J.J. Pankove, Optical Properties in Semiconductors, Prentice-Hall, Englewood Cliffs, NJ, 1971.
[70] K.A. Aly, J. Alloys Compd. 630 (2015) 178–182.
[71] A.A.M. Farag, M. Abdel Rafea, N. Roushdy, O. El-Shazly, E.F. El-Wahidy, J. Alloys Compd. 621 (2015) 434.
[72] D. Saritha, G. hikshamaiah, Intern. J. Eng. Res. 3 (2015) 140.
[73] I. Sharma, S.K. Tripathi, P.B. Barman, Appl. Surf. Sci. (2008).
[74] S.R. Elliott, The Physics and Chemistry of Solids, Wiley, Chichester, 2000.
[75] J.N. Zemel, J.D. Jensen, R.B. Schoolar, Phys. Rev. A 140 (1965) 330.
[76] J.A. Duffy, J. Phys, C Solid State Phys. 13 (1980) 2979–2989.
[77] R.R. Reddy, K.R. Gopal, K. Narasimhulu, L.S.S. Reddy, K.R. Kumar, C.V.K. Reddy, S.N. Ahmed, Opt. Mater. 31 (2008) 209.
[78] P. Heera, A. Kumar, R. Sharma, J. Ovonic Res. 8 (2) (2012) 29–40.
[79] V. Sadagopan, H.C. Gotos, Solid State Electron. 8 (1965) 529.
[80] H. Ticha, L. Tichy, N. Rysava, Trisha, J. Non-Cryst. Solids 354 (2008) 3468–3472.
[81] M.P. Sharma, N. Thakur, Philos. Mag. 89 (2009) 3027–3036.
[82] M.F. Thorpe, J. Non-Cryst. Solids 57 (1983) 355.
[83] A. Sharma, N. Mehta, Mater. Chem. Phys. 161 (2015) 35.
[84] L. Tichy, H. Ticha, Mater. Lett. 21 (1994) 313.
[85] R.J. F.reitas, K. Shimakawa, S. Kugler, Chalcogenide Lett. 10 (1) (2013) 39–43.